First-principles-informed energetic span and microkinetic analysis of ethanol catalytic conversion to 1,3-butadiene on MgO

Astrid Boje,[†] William E. Taifan,[‡] Henrik Ström,[¶] Tomáš Bučko,[§,‖] Jonas Baltrusaitis,[‡] and Anders Hellman[*,†,⊥]

†*Department of Physics, Chalmers University of Technology, 412 96 Göteborg, Sweden*

‡*Department of Chemical and Biomolecular Engineering, Lehigh University, B336 Iacocca Hall, 111 Research Drive, Bethlehem, PA 18015, USA.*

¶*Department of Mechanics and Maritime Sciences, Chalmers University of Technology, 412 96 Göteborg, Sweden*

§*Department of Physical and Theoretical Chemistry, Faculty of Natural Sciences, Comenius University in Bratislava, Ilkovičova 6, SK-84215, Bratislava, Slovak Republic*

‖*Institute of Inorganic Chemistry, Slovak Academy of Sciences, Dúbravská cesta 9, SK-84236 Bratislava, Slovak Republic*

⊥*Competence Centre for Catalysis, Chalmers University of Technology, 412 96 Göteborg, Sweden*

E-mail: anders.hellman@chalmers.se

Abstract

Kinetic modeling of single-step catalytic conversion of ethanol to 1,3-butadiene is necessary to inform accurate process design. This paper considers the synthesis of 1,3-butadiene on an MgO (100) step-edge using first-principles-informed energetic span and

microkinetic analysis to explore the reaction free energy landscapes and kinetic limitations of competing reaction pathways. Previous studies have observed mechanisms proceeding via both dehydrogenation and dehydration of ethanol, and highlighted sensitivity to conditions and catalyst composition. Here, we use the energetic span concept to characterize the theoretical maximum turnover and degree of rate control for states in each reaction pathway, finding dehydrogenation to be more active than dehydration for producing 1,3-butadiene, and suggesting states in the dehydrogenation, dehydration, and condensation steps to be rate-determining. The influence of temperature on the relative rate contribution of each state is quantified and explained through the varying temperature sensitivity of the free energy landscape. A microkinetic model is developed to explore the impact of competition between pathways, interaction with gas-phase species, and high surface coverage of stable reaction intermediates. This suggests that the turnover obtained may be significantly lower than predicted from the free energy landscape alone. The theoretical rate-determining states were found to contribute to high surface coverage of adsorbed ethanol and longer, oxygenated hydrocarbons. The combined energetic span and microkinetic analysis permits investigation of a complex system from two perspectives, each with inherent advantages, and helps elucidate conflicting observations of rate determining steps and product distribution by considering the interplay between the different pathways and the equilibrium with gas-phase products.

Keywords

energetic span, microkinetic model, ethanol-to-butadiene, MgO, heterogeneous catalysis

Introduction

Persistent and detrimental gas emissions from fossil fuel combustion stem from a range of societal drivers, including population and gross domestic product growth and the need for

continuous energy and commodity chemical supply.[1] As a result, recent research efforts on developing renewable and sustainable alternatives to petroleum for energy and commodity chemical production have been under rapid development.[2] (Bio)ethanol has been seen as an emerging platform molecule[3] to yield high-value chemicals and fuels[4,5] from cellulosic feedstock[6] that does not interfere with the food chain. Among the high-value chemicals obtained by catalytic transformation of (bio)ethanol is 1,3-butadiene (further in the text referred to as butadiene),[7] which has an established and widespread application in polymer synthesis and as an organic chemistry intermediate.[8] The conventional butadiene synthesis methods rely on steam cracking of naphtha or gas oil feedstocks. However, butadiene can also be recovered from olefinic refinery gases from the fluid catalytic cracker or, more recently, so called on-purpose butadiene synthesis from n-butane. For this reason, interest in the catalytic conversion of non-fossil fuel derived ethanol to butadiene via a single catalytic step, introduced in the 1930s by Lebedev,[9] has been revived and has focused on the development of selective catalysts to minimize the need for high-cost separations. The main components of the catalyst for this system are MgO and SiO_2.[10] Additionally, pure MgO and very high MgO content catalysts were also shown to be rather selective towards butadiene synthesis using specific preparation routes.[11,12] Noteworthy is that selectivity of the overall process has long been the limiting link as any improvements chiefly focused on the promotional effects of transition metals.

The lack of kinetic control over the single-step butadiene catalytic synthesis from ethanol and inadequate understanding of the fundamental mechanistic steps involved have hindered the development of catalysts with reasonable performance. The generally accepted one-step catalytic mechanism recently summarized by Pomalaza *et al.*[13] involves dehydrogenation of ethanol to acetaldehyde, which then undergoes C–C coupling via an aldol condensation mechanism to yield crotonaldehyde. Crotonaldehyde is further hydrogenated via MPV (Meerwein-Ponndorf–Verley) reduction with ethanol, and the resulting crotyl alcohol is dehydrated to form butadiene.[14,15] In addition, Fripiat and coworkers and Ostromislensky pro-

posed two other possible reaction pathways.[16,17] Fripiat suggested a Prins-like mechanism involving both dehydration and dehydrogenation reactions producing ethylene and acetaldehyde. The C=O group is hydroxylated in the presence of Brønsted acid and reacts with ethylene opening the double bond. The resulting 3-buten-2-ol is then dehydrated to yield butadiene.[17] Ostromislensky's version of the reaction mechanism involves the hemiacetal rearrangement between ethanol and acetaldehyde to yield 1-ethoxyethanol that later converts to butane-1,3-diol.[4]

Initial computational attempts using density functional theory under the generalized gradient approximation (GGA) by Zhang *et al.* focused on the dehydrogenation of the alcohol.[18] A stepped MgO surface was predicted to have a lower barrier than the flat surface for this reaction. Chieregato *et al.*, on the other hand, proposed an entirely different mechanism using cluster type calculations and Gaussian basis sets.[19] They ruled out crotonaldehyde and crotyl alcohol as possible intermediates and concluded that acetaldehyde would react with a carbanion resulting from ethanol C–H cleavage. The first comprehensive theoretical mechanism elucidation on MgO of ethanol catalytic coupling to butadiene used a kink Mg atom at a step-edge MgO (100) as a model catalyst surface in accordance with recent works[20–23] that suggest MgO as a bifunctional catalyst.[24–26] Another effort to elucidate the critical step in the C–C bond formation, i.e., aldol condensation, was undertaken on a metal-promoted surface and hydroxylated MgO surface,[27,28] with increased reactivity of hydroxylated MgO linked to modification of the basic properties of nearby active sites.[29] The surface proton back-transfer to 3-hydroxybutanal was shown to be more prominent when MgO is hydroxylated by ambient water vapor. Lower energetic barriers on the various aldol steps, i.e., enolization and C–C bond formation, were observed as well when the surface was promoted using Cu and Zr (not the focus of the current study). These changes brought about by water and transition metal promotion were attributed to the change in acidity and basicity of the MgO sites responsible in the reaction.[27,28] Despite its importance, the number of kinetic studies focusing on the reaction is limited. Da Ros *et al.* took a statistical approach by de-

coupling both measurement and catalytic reaction fluctuations on the microkinetic analysis of the system.[30] Very surprisingly, the covariance matrix of the composition measurements showed that the molar fraction variances were intercorrelated, and that the correlation patterns change with temperature. Microkinetic analysis of the correlation patterns led to the revelation that at 300 °C–400 °C, acetaldehyde condensation was the rate-determining step, while at 450 °C, ethanol dehydrogenation to acetaldehyde was shown to be the slowest step in the reaction.

The aim of the present study is to explore the contribution of competing pathways and the effect of conditions on the activity and selectivity of ethanol conversion to butadiene on an MgO (100) step-edge using energetic span (ES) and microkinetic (MK) analysis informed by first-principles calculations to obtain different perspectives on the dynamics. The reaction framework is based on the computational work of Taifan *et al.*, where low-coordinated MgO sites are used as the model catalyst.[24] The energetic span model is utilized to assess the efficiency of the catalyst cycles in terms of maximum turnover frequency (TOF) and to identify rate-determining states, using free energies derived from the first-principles calculations and accounting for temperature sensitivity in the entropic contributions to the free energy landscape. A microkinetic model is proposed to study competing pathways simultaneously and investigate kinetic limitations that may hinder the TOF achievable over realistic time-scales. Deviations of the modeling results from the energetic span theoretical predictions can be attributed to surface poisoning and competing reaction steps.

Results and discussion

Butadiene pathways and energetic span analysis

Four sequences of reaction steps were considered, based on the mechanism proposed by Taifan and coworkers.[24] For consistency, the same state labels will be used here where applicable so that it is possible to refer to the original structures and calculations. We supplemented these

calculations with additional transition states (states 3Fi and 6Gi, see Figs. S1 and S2 in the supporting information) for desorption of butadiene from C_4H_6O chemisorbed via two different functional groups, and with gas absorption data for hydrogen, water and acetaldehyde, all calculated using the same level of theory (see computational details). The surface and gas-phase molecules present in each state are documented in Tables S1–S3 and the electronic and free energies for the new states in Table S4 in the supporting information. All sequences involve the initial dehydrogenation of ethanol to acetaldehyde (path 1). Acetaldehyde formation can be followed by aldol condensation to yield 3-hydroxybutanal, and proton transfer resulting in crotonaldehyde (path 2) with MPV reduction resulting in 1,3-butadiene (path 3). Alternately, MPV reduction of 3-hydroxybutanal to adsorbed 1,3-butanediol and proton transfer yields 1,3-butadiene (path 4). Acetaldehyde formation, dehydration of ethanol to ethylene (path 5), and Prins condensation with proton transfer (path 6) is an alternative sequence by which 1,3-butadiene can be produced. Finally, a combination of acetaldehyde and adsorbed ethanol can form 1-ethoxyethanol, and subsequent molecular rearrangement could also yield 2-butenol (path 7). A combination of four different paths – 1, 2 and 3 (p123); paths 1, 2 and 4 (p124); paths 1, 5 and 6 (p156); or paths 1, 7 and 4 (p174) – can produce butadiene in this mechanism (Fig. 1). Depending on the particular sequence of reactions, however, the formation of several stable byproducts, such as acetaldehyde, crotonaldehyde, and ethylene, is also possible.

The free energy landscapes for each reaction sequence (Fig. 2 (a)–(c), also Fig. S4 (a) in the supporting information) were assembled from the free energies of each state and show varying degrees of sensitivity to temperature in the range 623 K–823 K. Temperature effects are introduced via entropic contributions to the free energy arising from translational, rotational, and vibrational degrees of freedom (equations 2–4 in the supporting information), where surface states are treated as fixed (no translational or rotational degrees of freedom). Increasing temperature typically corresponds to higher (or less negative) relative free energies of each state; however, in several states (i.e., 3D–3G, 4I–4K, 6A), increasing temperature

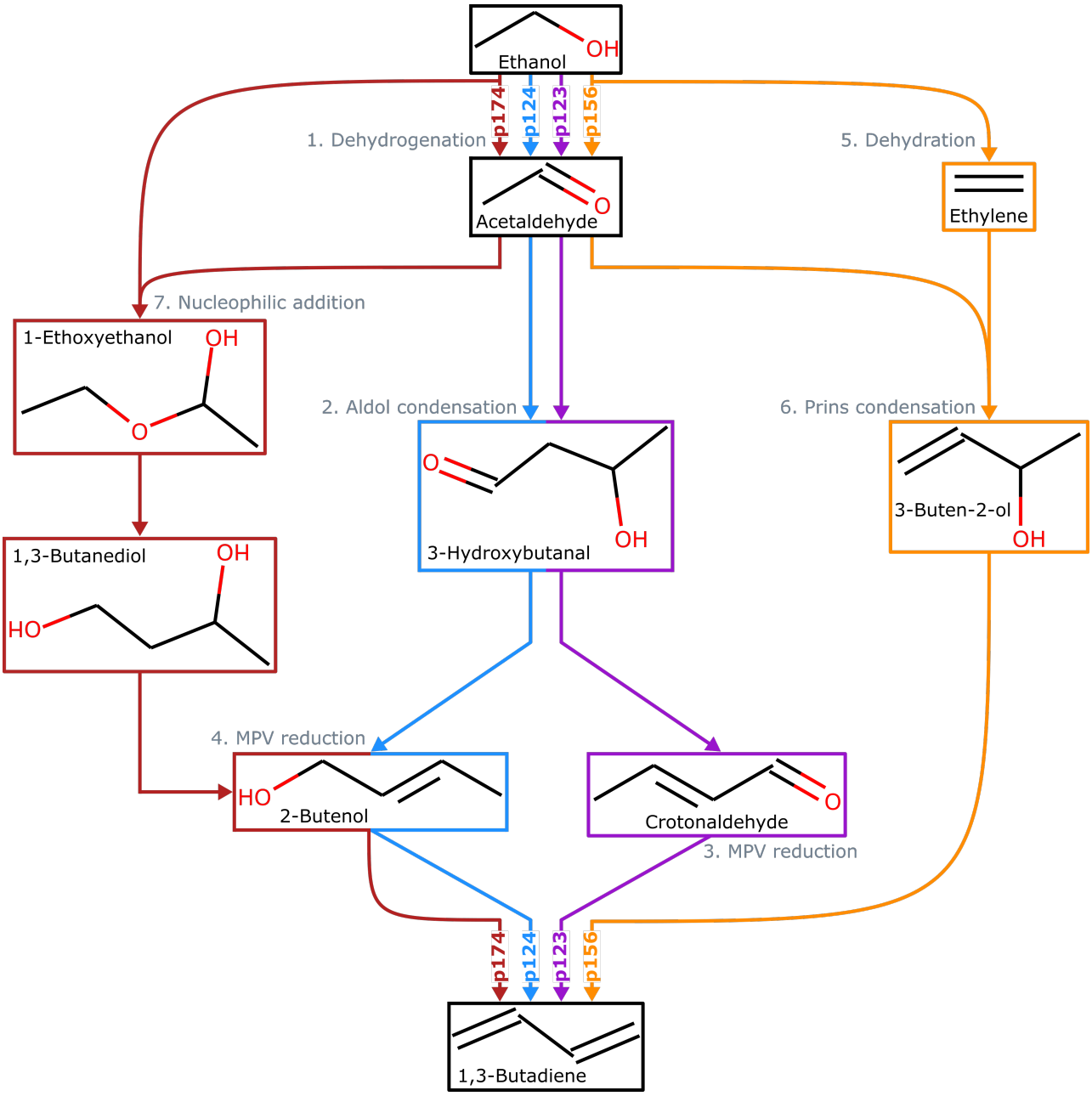

Figure 1: Key steps in each sequence of reactions leading from ethanol to butadiene formation. Numbers indicate paths. Arrows and intermediate blocks are colored by sequence. Sequences are labeled according to constituent paths: i.e., p123, p124, p156, and p174.

reduces the relative free energy thanks to the translational entropic contributions of the associated gas species (shown in Fig. S3 of the supporting information for two pairs of adjacent states for which the energy changes in opposing directions with temperature). Because of the states' different temperature sensitivities, the extent of the change in reaction energies (and barriers) with temperature is not uniform. It is important to account for this where possible, provided that there is sufficient confidence in the first-principles calculations for the effect to be significant (i.e., relative to the magnitude of the uncertainty in the energies). We studied the impact of uncertainty in the DFT data by perturbing the free energies with a zero-mean, $2\,\mathrm{kcal\,mol^{-1}}$ standard deviation, Gaussian noise and found that while individual predictions arising from the noisy data differed significantly (unsurprisingly, since the energies occur in the exponent in the rates), the average results were similar and consistent trends were observed (see Figs. S11–S16 and discussion in the supporting information).

The energetic span model proposed by Kozuch and Shaik[31] (see computational details) is a convenient tool to assess the theoretical performance of a catalyst cycle from the energetic information obtained from first-principles calculations. Its utility was recently demonstrated by Shylesh *et al.* studying ketonization of carboxylic acids and aldol condensation of propan-2-one over silica-supported zirconia, where C–C bond formation was found to be rate-limiting and reasonable agreement with experimental results was shown to be possible.[32] Garay-Ruiz and Bo have now presented a reaction-network-based implementation, applied to cobalt-catalyzed propene hydroformylation and copper-catalyzed hydrogenation of CO_2.[33]

The degree of rate control, X_{TOF}, for each transition state and intermediate (equations 3 and 4 in the computational details) was computed for each sequence at operationally relevant temperatures of 623 K, 723 K and 823 K, highlighting rate-determining intermediates (Fig. 2 (d)–(f), also Fig. S4 (b) in the supporting information) and transition states (Fig. 2 (g)–(i), also Fig. S4 (c) in the supporting information) for each sequence. Interestingly, the degree to which a state is rate-controlling varies with temperature, which agrees with findings by Da Ros *et al.* for MgO–SiO_2.[30] States 1A and 1B, which correspond to the

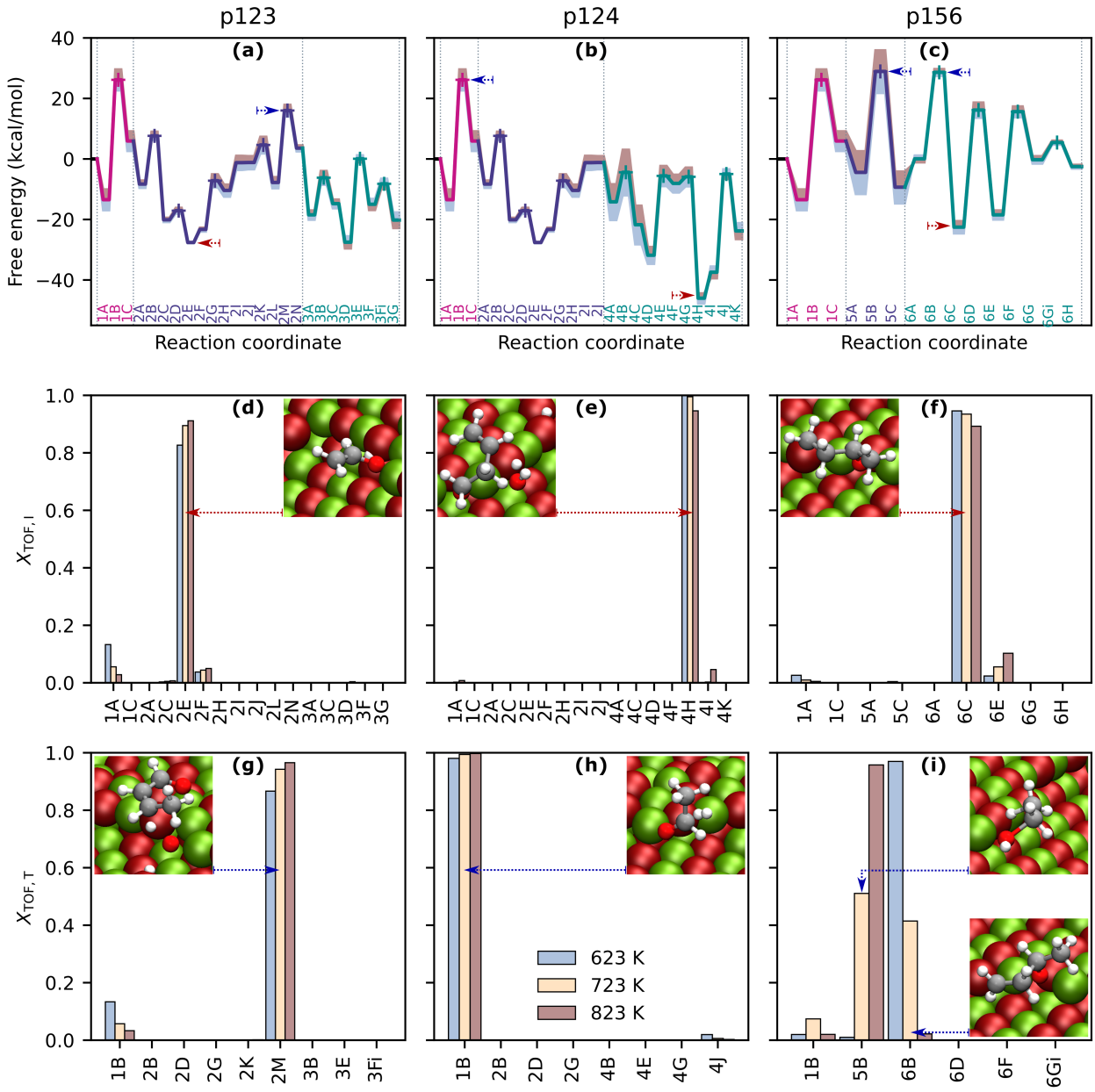

Figure 2: Pathway energy landscapes and rate controlling states. Panels (a)–(c): Free energy profiles for pathways p123, p124 and p156 at 723 K. Transition states labeled with + symbols. Effect of increasing (red) and decreasing (blue) temperature by 100 K indicated by filled regions. Molecules associated with each state are given in Tables S1 and S2. TDI and TDTS marked with red and blue dashed arrows. Panels (d)–(i): Energetic span assessment of relative TOF contributions of intermediates and transition states with insets showing states with maximum contributions.

initial and transition states for acetaldehyde formation from dissociatively adsorbed ethanol in the dehydrogenation path, are of greater importance to determining the TOF for p123 at 623 K than at 723 K and above, whereas states in the aldol condensation path become more significant with increasing temperature (Fig. 2 (d) and (g)). Temperature effects are even more significant for rate-determining transition states in p156, where transition state 5B, associated with the formation of ethylene from dissociatively adsorbed ethanol in the dehydration path, and transition state 6B, associated with the formation of C_4H_8O from acetaldehyde and ethylene in the Prins condensation path, are jointly rate controlling at 723 K but have almost no contribution at 623 K and 823 K, respectively (Fig. 2 (i)).

Transition state 1B from the ethanol dehydrogenation path is strongly rate-controlling at all relevant temperatures for p124 and p174, and is also slightly rate controlling for p123 and p156, for which the dominant transition states are 2M, associated with removal of atomic oxygen from $C_4H_6O_2$ in the aldol condensation path, and 5B/6B, respectively. Intermediate state 4H, including surface C_4H_7O, hydrogen, and hydroxide, from MPV reduction of 3-hydroxybutanal is rate-controlling for p124 and p174 (with a small contribution from 4I at high temperatures). For p123, the dominant intermediate is 2E (C_2H_3O), with small contributions from 1A (especially at low temperatures) and 2F (C_2H_3O and acetaldehyde). 6C (C_4H_8O) and, to a much smaller extent, 6E (C_4H_7O) and 1A are identified as rate-controlling intermediates for p156.

Because the contribution of energy differences to the rate is exponential, there is often only one significant energy difference between a stable intermediate and a hard-to-reach transition state. Where this is the case and the cycle is exergonic ($\Delta G_r < 0$), the TOF computation (equation 1 in the computational details) can be simplified to obtain an Arrhenius-type expression,[31] where the activation energy is the energetic span, δE, or energy difference between the turnover-determining transition state (TDTS) and turnover-determining intermediate (TDI), adding the reaction energy in the case where the TDTS appears before the TDI since these states occur in sequence across consecutive cycles.[31] This "energetic span

approximation" can be depicted visually by considering the free energy landscape across multiple catalyst cycles (Fig. 3, also Figs. S5–S7 in the supporting information) and finding the "largest hill to climb" between intermediates and transition states. Because the catalytic cycle ends at an energy displacement equal to the reaction energy, all states in the second cycle are altered by this quantity. For the dehydrogenation pathway with aldol condensation and MPV reduction of crotonaldehyde (p123), the TDI is state 2E and the TDTS is state 2M as discussed. The energetic span is 43.6 kcal mol^{-1} at 723 K. For the dehydrogenation path instead culminating in reduction of 3-hydroxybutanal (p124), the TDI is state 4H and the TDTS is state 1B – which occurs in the previous cycle (shaded zone spans two cycles in Fig. 3). Thus, the reaction energy of -23.8 kcal mol^{-1} must be included, yielding an energetic span of 48.4 kcal mol^{-1}. The situation for the path beginning with the molecular addition of acetaldehyde and ethanol (p174) is similar (Fig. S7 in the supporting information), but in this case, the reaction 1A–1C is followed by state 1A again, obtaining adsorbed ethanol and acetaldehyde as state 7A. Here, state 7E ($C_4H_9O_2$) is taken to be followed directly by state 4E ($C_4H_8O_2$ and H), ignoring the different structures of $C_4H_9O_2$ present in states 7E and 4D. The rate-determining intermediate and transition state are as in p124; thus, the energetic span is also the same. Finally, in the ethanol dehydration pathway (p156), there are two transition states with similar free energies at 723 K (Fig. S6). The energetic span is computed between intermediate state 6C and transition state 5B, across the catalytic cycle, and includes the relatively small reaction driving force of -2.51 kcal mol^{-1}, yielding a span of 49.0 kcal mol^{-1}.

The sequence with the smallest energetic span is p123. At 623 K, the largest is p124 and, at 723 K and above, it is p156 (Table 1). The predicted energetic spans for each pathway are 10 kcal mol^{-1}–20 kcal mol^{-1} larger than the apparent activation energy for butadiene production on silica-supported MgO reported by Taifan and coworkers under similar conditions.[34] The difference between the energetic spans of the extreme sequences is 7.3 kcal mol^{-1} at 623 K, 5.4 kcal mol^{-1} at 723 K and 9.2 kcal mol^{-1} at 823 K. The complete TOF expression

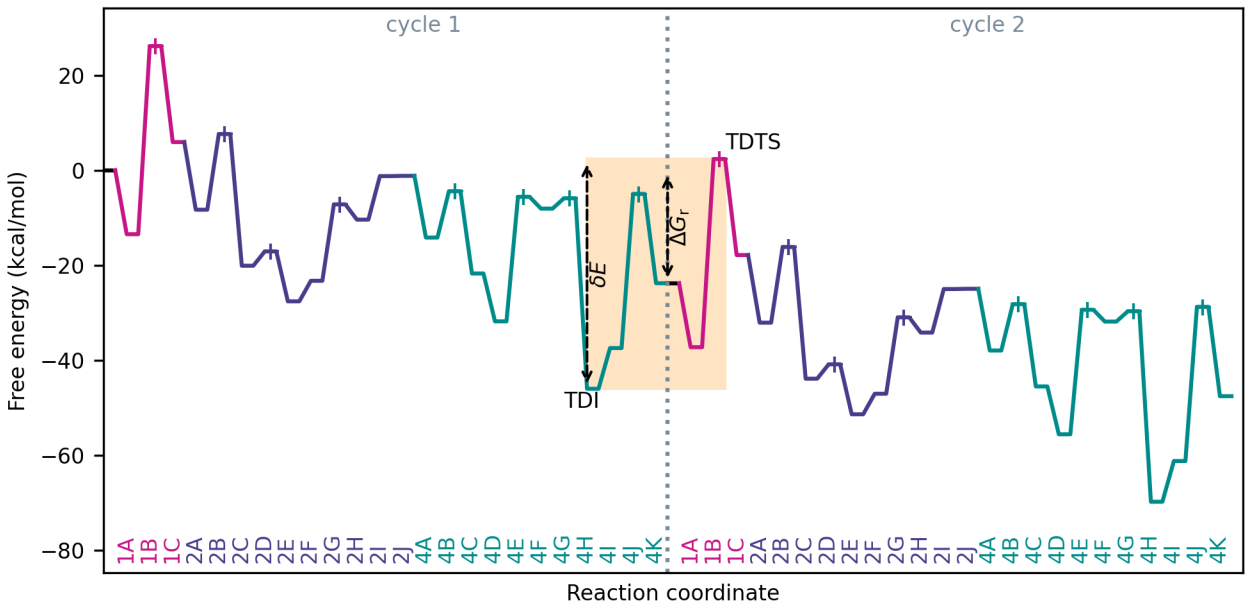

Figure 3: Graphical energetic span analysis for pathway p124 at 723 K. Dashed vertical arrows indicate reaction energy, ΔG_r, of one cycle and energetic span, δE, for TOF-determining transition state (TDTS) and intermediate (TDI). Transition states marked with + symbols.

(equation 1 in the computational details) was used to extend this analysis across a wider temperature range (Fig. 4). The sequence p123 was found to be most active over the whole temperature range, with a TOF one order of magnitude higher than the other sequences at most temperatures in the range 523 K–923 K. It is the only sequence with a predicted TOF near $1\,s^{-1}$ at 723 K. Only with a temperature of around 823 K, was the TOF from p124 also in this activity region. The TOF predicted for p156 was less than $0.1\,s^{-1}$ for all temperatures investigated; thus, we find that ethanol dehydrogenation should be more active in producing butadiene than dehydration. It is worth noting here that undoped MgO is not expected to be very active.[35,36] It is also instructive to compare the TOF profiles with the profiles obtained using constant free energies – those computed at 723 K (dotted lines on Fig. 4). This clearly illustrates the impact of temperature dependence due to the entropic contributions to the free energy landscape. Particularly for the dehydration pathway (p156), it is observed that there is a significant change in behavior when temperature dependence is accounted for, resulting in a greatly reduced TOF at temperatures above 723 K when

compared with the temperature-independent case. In principle, the energetic span analysis can be extended to consider competing pathways and influence of concentrations;[31] however, given the complexity of the pathways considered here, we will instead utilize microkinetic modeling to study these effects.

Table 1: Reaction energies, ΔG_{r}, and energetic spans, δE, for each reaction sequence.

Sequence	ΔG_{r} (kcal mol^{-1})			δE (kcal mol^{-1})		
	623 K	723 K	823 K	623 K	723 K	823 K
p123	-17.7	-20.2	-22.9	41.9	43.6	45.3
p124	-21.2	-23.8	-26.5	49.2	48.4	47.5
p156	-3.21	-2.51	-1.91	48.9	49.0	54.5
p174	-18.6	-18.0	-17.6	49.2	48.4	47.5

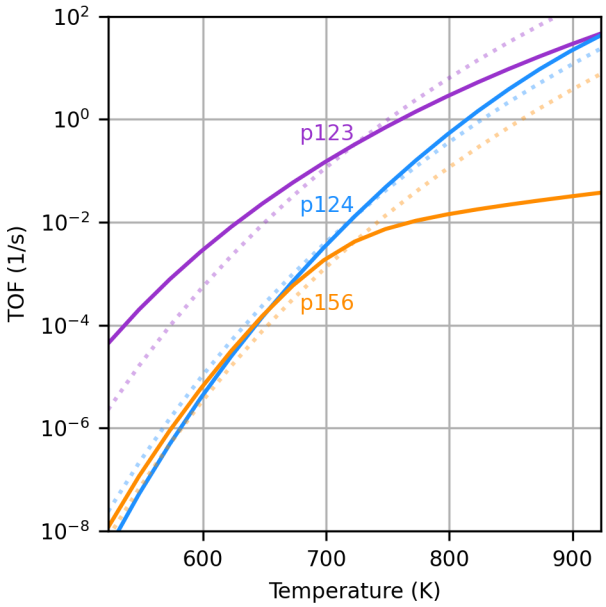

Figure 4: Energetic span predicted TOF for each pathway as a function of temperature. State free energies were calculated accounting for temperature dependence of the entropic contributions, resulting in leveling off at high temperatures. Dotted lines show TOFs calculated with state free energies calculated at 723 K.

Microkinetic model for butadiene mechanism

In order to consider all pathways simultaneously and investigate coverage limitations and composition effects, we now turn to microkinetic modeling of the surface dynamics (imple-

mentation discussed in the computational details). For each step, 1A–1C, 2A–2C, etc., a reaction describing the change from initial to final states was formulated using the same free energy landscape as in the energetic span analysis, but ignoring distant surface molecules not directly involved in reactions, and steps involving diffusion. Reaction rate expressions were formulated assuming the law of mass action applies (steps and rates are provided in Table S7 of the supporting information). Adsorption and desorption kinetics were included for gas-phase species, including hydrogen, water, acetaldehyde, crotonaldehyde, and ethanol. Ethylene and butadiene were assumed to react from the gas-phase without surface adsorption. Lone surface oxygen and hydrogen atoms were allowed to combine to form hydroxide. Table S6 in the supporting information lists the reaction barriers and energies at 623 K–823 K, and Table S8 in the supporting information provides the differential equations for transient coverage of each surface species.

Under most conditions, the TOF realized by the microkinetic model was found to be significantly lower than the theoretical maximum predicted by energetic span theory for the individual pathways (Fig. 5). This is unsurprising as the energetic span analysis did not account for coverage limitations or interaction with the gas-phase. For a system at 2 kPa ethanol partial pressure with roughly 1 % hydrogen and ethylene and trace amounts of other gas-phase species (ensuring all steps can occur bidirectionally), high surface coverage rapidly developed with transient dominance of several species indicating the influence of the different pathways. Initially, adsorbed ethanol and hydrogen were the most prevalent species at all three temperatures (Fig. 6); however, surface coverage rapidly evolved in favor of two four-carbon species – $C_4H_9O_2$, formed in the dehydrogenation pathway (p124), and C_4H_8O, formed in the dehydration pathway (p156). At 723 K, similar coverage fractions of both species were obtained after 24 h online. At the lower and higher temperatures, more significant fractions of the p124 and p156 intermediates were observed, respectively. The presence of strongly-bound intermediates has been observed experimentally under similar conditions, for example by Abdulrazzaq *et al.* who also found that the apparent activation

energy for dehydrogenation was lower than that for dehydration and suggested the low apparent barrier for dehydrogenation was linked to the abundance of a stable surface species.[37] Strongly-bound surface species were also observed with *in situ* spectroscopy (DRIFTS) by Taifan *et al.*, with identified species including adsorbed ethanol/ethyoxy, acetaldehyde, aldol condensation and polymerization products, and C_4 species such as butanol and crotyl alcohol.[25,34] Hayashi *et al.* reported significant quantities of oxygenates and longer hydrocarbons on MgO and a rate two orders of magnitude lower than for MgO doped with Zn.[38]

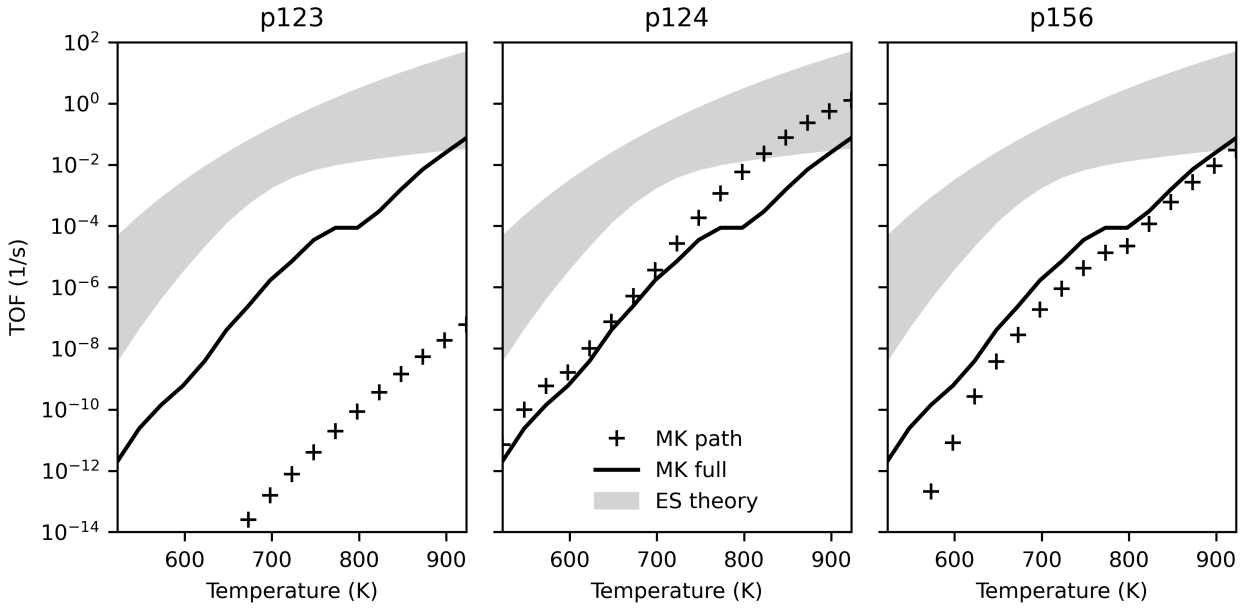

Figure 5: TOF comparison for energetic span (ES) theory and microkinetic (MK) model as a function of temperature. Filled regions illustrate turnover range predicted by ES theory for each pathway; solid lines show TOF achieved by MK model with all pathways active; and markers indicate TOF achieved by MK model considering only individual pathways. The partial pressures of ethanol, hydrogen and ethylene were 2 kPa, 0.02 kPa and 0.02 kPa with trace amounts (2×10^{-8} kPa) of other gases, and a total pressure of 101.3 kPa.

Ethanol dehydrogenation followed by aldol condensation and MPV reduction of crotonaldehyde (p123) was predicted by the energetic span theory to be somewhat limited by the initial acetaldehyde formation (due to stability of adsorbed ethanol – state 1A) but the TOF was expected to be primarily determined by the stable intermediate state 2E (C_2H_3O) and the transition state 2M ($C_4H_6O_2$). Interestingly, the conditions investigated here resulted

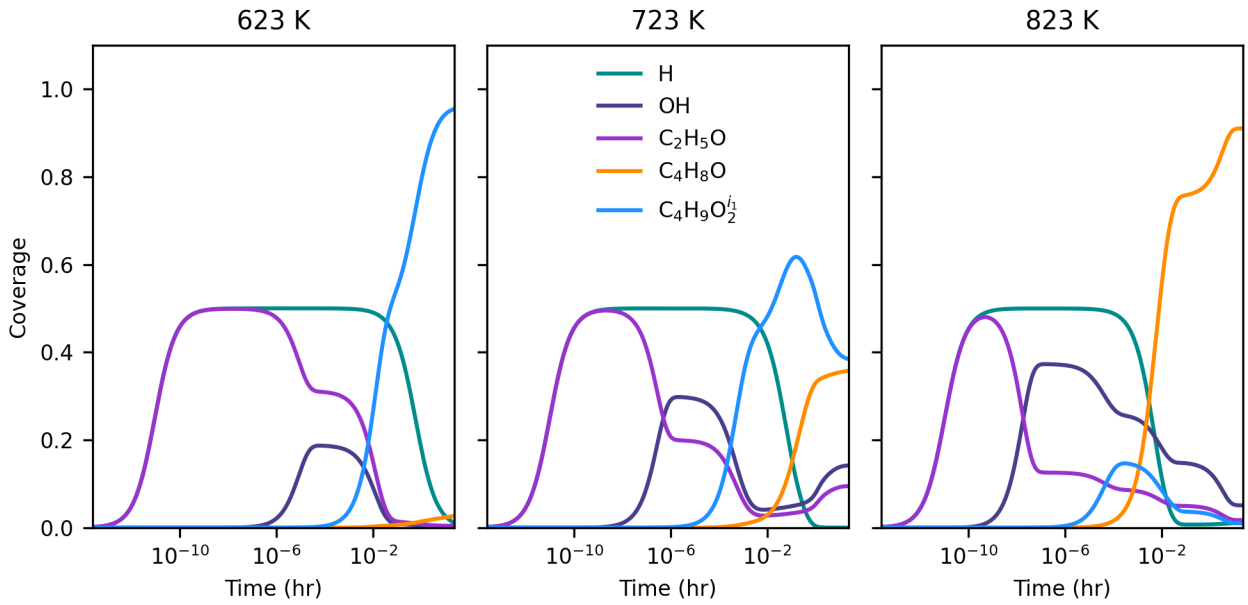

Figure 6: Transient surface coverage of dominant species. Only species with maximum coverage greater than 2% drawn. The partial pressures of ethanol, hydrogen and ethylene were 2 kPa, 0.02 kPa and 0.02 kPa with trace amounts (2×10^{-8} kPa) of other gases, and a total pressure of 101.3 kPa.

in rapid, more favorable desorption of acetaldehyde, and the turnover obtained for p123 was consequently much lower than predicted by the ES analysis (Fig. 5, markers in left panel versus top of filled region). Surface coverage for p123 only (Fig. S8 in the supporting information) was found to be dominated by adsorbed ethanol, with a flux of ethanol to acetaldehyde, a trace amount of crotonaldehyde, and hydrogen (Fig. 7). By comparison, ethanol dehydration followed by aldol condensation and MPV reduction of 3-hydroxybutanal (p124) was found to be a relatively active pathway, with turnover in the predicted region at high temperatures (Fig. 5, center panel – note that the obtained TOF was still lower than the theoretical maximum predicted for p124 shown in Fig. 4 which is to be expected). For p124, the energetic span theory predicted that state 4H (C_4H_7O) would be rate limiting. However, this state is preceded by another significantly stable state, 4D ($C_4H_9O_2$), and this species was found to dominate surface coverage in the first 24 h (Fig. S9 in the supporting information), possibly owing to the low concentration of free sites needed to deprotonate it

via 4D–F. Again, most ethanol was converted to acetaldehyde; however, around ten percent of the adsorbing carbon was converted to butadiene. High acetaldehyde selectivity relative to ethylene – greater than 80 % at 723 K with ethanol partial pressure less than 10 kPa and 101.3 kPa total pressure – has also been observed experimentally for a model MgO/SBA-15 catalyst.[37]

The TOF for ethanol dehydration and Prins condensation (p156) was predicted by the ES analysis to be determined by the stability of state 6C (C_4H_8O) and the barriers to reach transition states 5B and 6B (depending on temperature). The kinetic model found surface coverage to be mostly C_4H_8O, with early significance of adsorbed ethanol as well as hydroxide (Fig. S10 in the supporting information). As with the other pathways, the TOF was lower than predicted by the ES theory (Fig. 5, right panel) and ethanol was predominantly converted to acetaldehyde with approximately 2 % ethylene and 2 % butadiene. Because the pathways compete, the overall TOF obtained by the microkinetic model was found to be lower than the TOF obtained with only p124, although it is higher than the individual TOFs of both p123 and p156. Also noteworthy is the relative impact of the pathways as a function of temperature – the kink in the TOF profile for the full MK model at around 800 K (Fig. 5) corresponds to changing surface coverage in favor of p156 intermediate C_4H_8O from p124 intermediate $C_4H_9O_2$ (Fig. 6), and more significant influence of p156 compared to p124. By comparison, the energetic span analysis predicted a leveling-off of the turnover for p156 by around 800 K.

The studies discussed above highlight the challenge of improving selectivity for ethanol conversion to butadiene due to the competitive formation of other products – here, acetaldehyde and crotonaldehyde (Fig. 7), but experiments have found significant quantities of ethylene[34] and lesser quantities of other species such as crotyl alcohol, butenes and longer hydrocarbons.[11,30] Selectivity towards crotonaldehyde was found to be low here due to more favorable consumption of the acetaldehyde by aldol condensation in p124 and its desorption from the surface before p123 can progress to the crotonaldehyde formation stage. For the

system with non-negligible hydrogen and ethylene pressures and trace quantities of other species, the 2 kPa ethanol partial pressure at 723 K appears to be a reasonably selective setting for butadiene formation (Fig. 8), yielding almost 25 % of butadiene in a predominantly acetaldehyde containing mixture. For reference, Da Ros *et al.*[30] obtained a butadiene yield of around 20 % at 723 K on 95:5 MgO–SiO_2 and Taifan *et al.*[26] reported up to 30 % selectivity for butadiene under similar conditions, but with significantly more ethylene formation. At higher temperatures, more ethylene was formed (but still under 10 %). Zhu *et al.* also observed increasing ethylene with temperature and maximal butadiene selectivity at 723 K.[39] Water formation has been observed experimentally,[25] and was found to occur to a small extent in the current study (Fig. 7).

Conclusions

Two theoretical methods were compared for the activity and selectivity of butadiene formation from ethanol. Energetic span theory provides an efficient estimate of the maximum achievable turnover across catalytic cycles for a single reaction pathway and can identify turnover-determining stable intermediates (TDI) and difficult to reach transition states (TDTS) from first-principles energies of each state in the pathway. Here, energetic span theory calculations for individual pathways predicted that ethanol dehydrogenation and aldol condensation can achieve a higher turnover than dehydration, followed by Prins condensation. Even so, the predicted turnover was found to be less than $1\,s^{-1}$ for all pathways and temperatures investigated here at 723 K, in line with experimental observations that pure MgO surfaces are only weakly active towards butadiene production. The energetic span analysis indicated that the rate of butadiene formation would be determined by intermediate states involving adsorbed ethanol, C_2H_3O, C_4H_7O, and C_4H_8O with hydrogen, as well as transition states associated with acetaldehyde and crotonaldehyde formation.

The entropic contributions to the states' free energies were calculated at each temper-

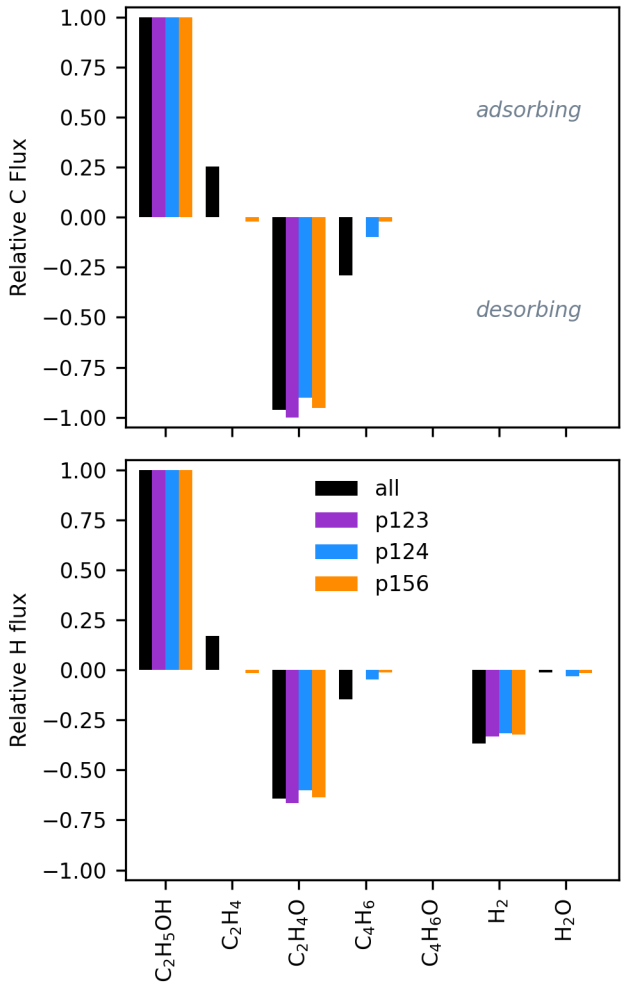

Figure 7: Elemental flux after 24 h operation. The partial pressures of ethanol, hydrogen and ethylene were 2 kPa, 0.02 kPa and 0.02 kPa, respectively, with trace amounts of other products (2×10^{-8} kPa), and a total pressure of 101.3 kPa.

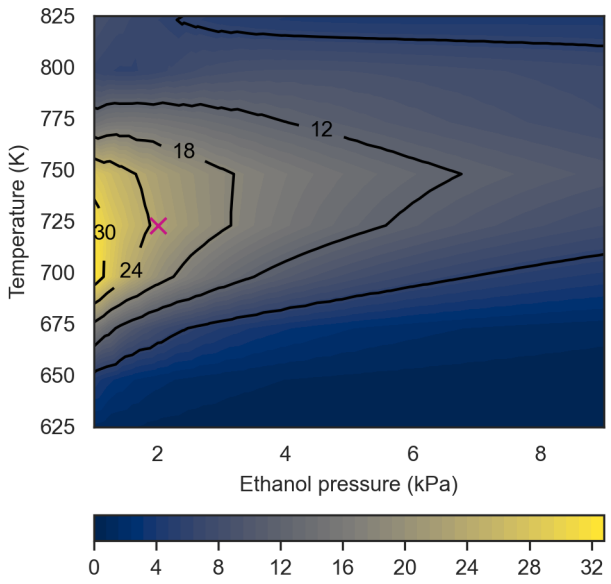

Figure 8: Butadiene selectivity as a function of ethanol partial pressure and temperature after 24 h operation. Marker indicates conditions used in other results figures. The partial pressures of hydrogen and ethylene were 0.02 kPa with trace amounts of other products (2×10^{-8} kPa), and a total pressure of 101.3 kPa. Selectivity is defined as the flux from all adsorbing carbon to desorbing butadiene.

ature investigated in this work, to account for temperature effects across the energy landscape. Temperature was found to have a significant effect on entropic contributions of some states, especially those with associated gas molecules, as their translational contributions can change significantly. The variation in the energy landscape with temperature is consequently non-uniform because some binding energies (and thus barriers) change more than others. This leads to varying significance of different states at high or low temperatures; for example, in the ethanol dehydration pathway, different transition states were found to be rate-determining at 623 K and 823 K, with a combination of the two being important at 723 K. Another consequence is that the predicted TOFs do not all follow the same trajectory with increasing temperature. This leads to varying importance of the entire pathway's contribution when the pathways are viewed together, motivating microkinetic modeling for further analysis.

A microkinetic model was developed to consider the impact of multiple pathways on

the butadiene formation rate and selectivity. This provides important insight that is not possible from the theoretical energetic analysis alone as it accounts for competition between sequences of reaction steps, surface poisoning over long, but finite times, and impact of adsorption/desorption equilibria on surface availability of reaction intermediates (i.e. various forms of kinetic limitations). Microkinetic modeling of each pathway individually suggested that it is difficult to achieve a turnover in the range predicted by the energetic span model due to the kinetic limitations at finite times/temperatures. The ethanol dehydrogenation and aldol condensation pathway with MPV reduction of 3-hydroxybutanal (p124) yields a TOF in the range predicted for the individual pathways; however, the TOF obtained for the pathway with reduction of crotonaldehyde (p123) was found to be significantly lower than predicted due to more favorable desorption of acetaldehyde.

When the pathways were modeled together, the TOF obtained was higher than for the first dehydrogenation pathway (p123) or the dehydration pathway (p156), due to the dominance of the second dehydrogenation pathway (p124), especially in the lower temperature range where the surface coverage was predominantly a p124 intermediate – $C_4H_9O_2$. In general, surface coverage for each pathway was found to be very high – with rate-determining intermediate states from the theoretical predictions observed to be prevalent in some cases. In addition to adsorbed ethanol, hydrogen, and some hydroxide, $C_4H_9O_2$ from p124 and C_4H_8O from p156 dominate surface coverage under the conditions explored here. A change in dynamics is noticeable at around 800 K, where the TOF slope changes and the surface coverage shifts in favor of C_4H_8O. The current model does not allow the $C_4H_9O_2$ isomer formed in path 7 (by nucleophilic addition of ethanol and acetaldehyde) to rearrange to form the isomer used in path 4 as the energy landscape for this process was not readily available and it would likely lead to dissociation of the molecule.[24] The microkinetic modeling results find that surface coverage of the path 7 $C_4H_9O_2$ species is negligible, suggesting that this pathway is not a significant route to the production of butadiene.

The conditions investigated here could achieve a maximum selectivity of just under 25 %,

with the remainder of the adsorbing carbon predominantly desorbing as acetaldehyde with trace amounts of crotonaldehyde. Ethylene flux leaving the surface was only observed at temperatures approaching 800 K and above. These results are sensitive to variation in temperature and ethanol partial pressure – thus, conditions are expected to have a substantial impact on the turnover and selectivity obtained. In general, performance will vary with both conditions and catalyst preparation/composition.[11] MgO studied experimentally is typically supported by silica (and often doped to improve selectivity and activity). Here, we have assumed that the MgO step-edge is a suitable model catalyst system, but it is worth noting that this approach cannot resolve variations in performance arising from the quantity of silica added or the synthesis conditions – which have been suggested to affect the ratio and strength of acidic and basic sites.[40] It is anticipated that inclusion of dopant atoms such as copper or zinc in the energetic calculations would result in a higher turnover prediction[4] by the kinetic modeling. Mean-field modeling is, of course, not without limitations. It is worth noting that the current model ignores differences between sites when considering adsorbates. The mechanism is also truncated at four-carbon intermediate species, where there is evidence of polymerization to longer carbon chains over long periods online.[25,38] Despite these caveats, the first-principles-informed microkinetic model allows useful insight into a complex catalytic system and provides an interesting kinetics-informed comparison with predictions derived from theoretical analysis of the thermodynamic limiting behavior of this system.

Computational details

Electronic structure and free energy calculations

Most of the electronic energies used in this paper were taken from the first-principles study of Taifan *et al.*[24], in which the DFT calculations were performed using VASP[41–44] where the projector augmented wave method[45] was employed to reduce the number of basis functions necessary to describe the wave function. The Kohn-Sham orbitals were represented in a

plane-wave basis set with a cutoff of 400 eV. The PBE generalized gradient approximation[46] was used to represent the exchange-correlation potential. Brillouin-zone sampling was performed with a $2 \times 2 \times 1$ k-point mesh. The self-consistent field convergence criterion was set to 10^{-6} eV per cell total energy change. Transition states were located using the improved version[47] of the dimer method.[48] Atomic positions were relaxed until the forces on all atoms were less than $0.005\,\mathrm{eV\,\AA^{-1}}$. The correctness of vibrational spectra of all stationary points (in particular, the number of zero and imaginary frequencies) was verified.

All surface computations were performed using a periodic, three layer magnesium oxide (MgO) slab consisting of $8 \times 6 \times 3$ primitive cells with the atoms in the bottom layer fixed in position while the other layers were allowed to relax. The PBE lattice parameter was calculated to be 4.255 Å. The Mg_{3C} coordinated with O_{4C} stepped kink sites were taken to be the active sites for reaction. Isolated gas computations were performed using a $10 \times 10 \times 10$ $\mathrm{\AA}^3$ cell.

Several additional states were required to support the theoretical and numerical analysis in the current work, and these were computed using the same stepped MgO surface, level of theory and method. Two transition states (3Fi and 6Gi) were computed for desorption of butadiene from C_4H_6O chemisorbed by the terminal CH_2 and the CH groups. Here, the transition states were computed using the nudged elastic band (NEB) method.[49,50] Energies were also computed for hydrogen, water and acetaldehyde adsorption and hydroxide dissociation. Data for these states is provided in the supporting information.

The free energies used here were computed using the rigid-rotor harmonic-oscillator approximation to transition state theory[51] with electronic energies from DFT and temperature-dependent translational, vibrational, and rotational contributions as described in the supporting information. Relative energies were referenced to the sum of the relaxed MgO slab and three non-interacting gas-phase molecules of ethanol.

Energetic span calculations

The energetic span model presented by Kozuch and Shaik[31] provides a theoretical means to assess the efficiency of catalytic cycles in terms of turnover frequency (TOF) using the state energies derived from first-principles calculations. The reaction energy landscape is characterized using the energy differences between intermediate–transition state pairs and the reaction driving force, i.e., the energy change across one catalytic cycle. The TOF can be computed by summation of pairwise energy differences for all states,

$$\mathrm{TOF} = \frac{k_\mathrm{B}T}{h}\frac{e^{-\Delta G_\mathrm{r}/RT}-1}{\sum_{ij} e^{\left(G_{T_i}-G_{I_j}-\delta G_{ij}\right)/RT}}, \tag{1}$$

where the summation is taken over all transition states (T) and reaction intermediates (I) occurring within the catalytic cycle. Indexing the states T by i and I by j, the term δG_{ij} is defined as follows:

$$\delta G_{ij} = \begin{cases} \Delta G_\mathrm{r} & i > j \\ 0 & i \leq j. \end{cases} \tag{2}$$

Note that Kozuch and Shaik identified the first intermediate with index $j = 0$ and the first transition state with index $i = 1$. Implementing this with indexing starting at zero for both sets of states instead corresponds to the inequality condition $i \geq j$ for δG_{ij}. Similar to the degree of rate control[52,53] typically used to identify rate determining steps, the energetic span model uses the pairwise energy differences between states to investigate the degree of TOF control of transition states,

$$X_{\mathrm{TOF,T}_i} = \frac{\sum_j e^{\left(G_{T_i}-G_{I_j}-\delta G_{ij}\right)/RT}}{\sum_{ij} e^{\left(G_{T_i}-G_{I_j}-\delta G_{ij}\right)/RT}}, \tag{3}$$

and intermediates,

$$X_{\mathrm{TOF,I}_j} = \frac{\sum_i e^{\left(G_{T_i}-G_{I_j}-\delta G_{ij}\right)/RT}}{\sum_{ij} e^{\left(G_{T_i}-G_{I_j}-\delta G_{ij}\right)/RT}}. \tag{4}$$

and find rate determining states in the cycle. The degree of TOF control identifies a turnover-determining transition state (TDTS) and a turnover-determining intermediate (TDI), which are not necessarily the highest and lowest points on the free energy landscape, or adjacent states, but represent the largest energy difference across successive catalytic cycles. This analysis can be extended to consider the influence of reactants and products on the TOF.[54] Because the TOF is linearly proportional to concentrations, excluding trace or excess concentration cases, only species located between the TDI and TDTS can accelerate or inhibit the overall reaction. The energetic span calculations identifying the TOF, X_{TOF}, TDTS and TDI were implemented in Python using equations 1–4.

Microkinetic model

The microkinetic model (Table S7) was constructed with consideration of the mechanistic steps presented in Taifan and coworkers[24], neglecting all spectator surface species (typically hydrogen) that are unlikely to participate in the reaction but including species that may catalyze certain steps. Proton diffusion steps were neglected. Isomers were treated as distinct species. The mechanism was supplemented by further chemistry for oxygen and hydrogen, adsorption/desorption equilibria for H_2, H_2O, acetaldehyde and crotonaldehyde, as well as transition states for butadiene formation from dissociative desorption of C_4H_6 from two C_4H_6O structures. The initial and final states for these dissociative desorption events were identified by Taifan *et al.*[24] and the transition states were computed in the current work. The resulting system of ordinary differential equations (Table S8) was solved in MATLAB 2018a, using the stiff ODE solver *ode23s* with backwards difference formulas (BDF), and relative and absolute tolerances of 10^{-6} and 10^{-8}, respectively. An analytic expression was derived for the Jacobian and provided to the solver. Further details are provided in the supporting information.

Acknowledgement

This work was supported by the Knut and Alice Wallenberg Foundation (Project 2015.0057), the Swedish Research Council (Project 2015-03773) and the National Science Foundation under Grant No. CHE 1710120. This work used the Extreme Science and Engineering Discovery Environment (XSEDE),[55] which is supported by the National Science Foundation grant number ACI-1053575. Computational resources were provided by the Swedish National Infrastructure for Computing (SNIC) at C3SE (Gothenburg) and NSC (Linköping).

Supporting Information Available

Periodic structures of all surface states. Molecular composition of all states, energies of states introduced in this work, free energy contributions from translational, rotational and vibrational degrees of freedom, reaction barriers and energies, energetic span analysis for other pathways, microkinetic model steps, rate equations and coverages for each pathway.

References

(1) Luderer, G. et al. Residual fossil CO_2 emissions in 1.5–2 °C pathways. *Nature Climate Change* **2018**, *8*, 626–633.

(2) Ragauskas, A. J.; Williams, C. K.; Davison, B. H.; Britovsek, G.; Cairney, J.; Eckert, C. A.; Frederick, W. J.; Hallett, J. P.; Leak, D. J.; Liotta, C. L.; Mielenz, J. R.; Murphy, R.; Templer, R.; Tschaplinski, T. The Path Forward for Biofuels and Biomaterials. *Science* **2006**, *311*, 484–489.

(3) Posada, J. A.; Patel, A. D.; Roes, A.; Blok, K.; Faaij, A. P.; Patel, M. K. Potential of bioethanol as a chemical building block for biorefineries: Preliminary sustainability

assessment of 12 bioethanol-based products. *Bioresource Technology* **2013**, *135*, 490–499.

(4) Angelici, C.; Weckhuysen, B. M.; Bruijnincx, P. C. A. Chemocatalytic Conversion of Ethanol into Butadiene and Other Bulk Chemicals. *ChemSusChem* **2013**, *6*, 1595–1614.

(5) Sun, J.; Wang, Y. Recent Advances in Catalytic Conversion of Ethanol to Chemicals. *ACS Catalysis* **2014**, *4*, 1078–1090.

(6) Robertson, G. P.; Hamilton, S. K.; Barham, B. L.; Dale, B. E.; Izaurralde, R. C.; Jackson, R. D.; Landis, D. A.; Swinton, S. M.; Thelen, K. D.; Tiedje, J. M. Cellulosic biofuel contributions to a sustainable energy future: Choices and outcomes. *Science* **2017**, *356*.

(7) Pomalaza, G.; Capron, M.; Ordomsky, V.; Dumeignil, F. Recent Breakthroughs in the Conversion of Ethanol to Butadiene. *Catalysts* **2016**, *6*, 203.

(8) Srivastava, V. K.; Sarkar, S. S. P.; Rao, G. S.; Jasra, R. V. Industrial Chemicals and Intermediates from 1,3-Butadiene. *Recent Advances in Petrochemical Science* **2018**, *6*, 555698.

(9) Lebedev, S. V. Preparation of bivinyl directly from alcohol. I. *Zh Obshch Khim* **1933**, 698–717.

(10) Makshina, E. V.; Dusselier, M.; Janssens, W.; Degrève, J.; Jacobs, P. A.; Sels, B. F. Review of old chemistry and new catalytic advances in the on-purpose synthesis of butadiene. *Chemical Society Reviews* **2014**, *43*, 7917–7953.

(11) Hayashi, Y.; Akiyama, S.; Miyaji, A.; Sekiguchi, Y.; Sakamoto, Y.; Shiga, A.; Koyama, T.-r.; Motokura, K.; Baba, T. Experimental and computational studies of the roles of MgO and Zn in talc for the selective formation of 1,3-butadiene in the conversion of ethanol. *Physical Chemistry Chemical Physics* **2016**, *18*, 25191–25209.

(12) Reschetilowski, W.; Hauser, M.; Alscher, F.; Klauck, M.; Kalies, G. Studies on the Binary MgO/SiO_2 Mixed Oxide Catalysts for the Conversion of Ethanol to 1,3-Butadiene. *Catalysts* **2020**, *10*.

(13) Pomalaza, G.; Arango Ponton, P.; Capron, M.; Dumeignil, F. Ethanol-to-butadiene: the reaction and its catalysts. *Catalysis Science & Technology* **2020**, *10*, 4860–4911.

(14) Quattlebaum, W. M.; Toussaint, W. J.; Dunn, J. T. Deoxygenation of Certain Aldehydes and Ketones: Preparation of Butadiene and Styrene1. *Journal of the American Chemical Society* **1947**, *69*, 593–599.

(15) Toussaint, W. J.; Dunn, J. T.; Jachson, D. R. Production of Butadiene from Alcohol. *Industrial & Engineering Chemistry* **1947**, *39*, 120–125.

(16) Ostromuisslenskii, I. I. New methods of preparing of erythrene. *Zh. Russ. Fiz.-Khim. O-va.* **1915**, *47*, 1472–94.

(17) Gruver, V.; Sun, A.; Fripiat, J. J. Catalytic properties of aluminated sepiolite in ethanol conversion. *Catalysis Letters* **1995**, *34*, 359–364.

(18) Zhang, M.; Gao, M.; Chen, J.; Yu, Y. Study on key step of 1,3-butadiene formation from ethanol on MgO/SiO_2. *RSC Advances* **2015**, *5*, 25959–25966.

(19) Chieregato, A.; Velasquez Ochoa, J.; Bandinelli, C.; Fornasari, G.; Cavani, F.; Mella, M. On the Chemistry of Ethanol on Basic Oxides: Revising Mechanisms and Intermediates in the Lebedev and Guerbet reactions. *ChemSusChem* **2015**, *8*, 377–388.

(20) Bailly, M.; Chizallet, C.; Costentin, G.; Kraft, J.; Lauronpernot, H.; Che, M. A spectroscopy and catalysis study of the nature of active sites of MgO catalysts: Thermodynamic Brønsted basicity versus reactivity of basic sites. *Journal of Catalysis* **2005**, *235*, 413–422.

(21) Chizallet, C.; Costentin, G.; Che, M.; Delbecq, F.; Sautet, P. Revisiting Acido-basicity of the MgO Surface by Periodic Density Functional Theory Calculations: Role of Surface Topology and Ion Coordination on Water Dissociation. *The Journal of Physical Chemistry B* **2006**, *110*, 15878–15886.

(22) Branda, M. M.; Rodríguez, A. H.; Belelli, P. G.; Castellani, N. J. Ethanol adsorption on MgO surface with and without defects from a theoretical point of view. *Surface Science* **2009**, *603*, 1093–1098.

(23) Cornu, D.; Guesmi, H.; Krafft, J.-M.; Lauron-Pernot, H. Lewis Acido-Basic Interactions between CO_2 and MgO Surface: DFT and DRIFT Approaches. *The Journal of Physical Chemistry C* **2012**, *116*, 6645–6654.

(24) Taifan, W. E.; Bučko, T.; Baltrusaitis, J. Catalytic conversion of ethanol to 1,3-butadiene on MgO: A comprehensive mechanism elucidation using DFT calculations. *Journal of Catalysis* **2017**, *346*, 78–91.

(25) Taifan, W. E.; Yan, G. X.; Baltrusaitis, J. Surface chemistry of MgO/SiO_2 catalyst during the ethanol catalytic conversion to 1,3-butadiene: in-situ DRIFTS and DFT study. *Catalysis Science & Technology* **2017**, *7*, 4648–4668.

(26) Taifan, W. E.; Baltrusaitis, J. In Situ Spectroscopic Insights on the Molecular Structure of the MgO/SiO_2 Catalytic Active Sites during Ethanol Conversion to 1,3-Butadiene. *The Journal of Physical Chemistry C* **2018**, *122*, 20894–20906.

(27) Fan, D.; Dong, X.; Yu, Y.; Zhang, M. A DFT study on the aldol condensation reaction on MgO in the process of ethanol to 1,3-butadiene: understanding the structure–activity relationship. *Physical Chemistry Chemical Physics* **2017**, *19*, 25671–25682.

(28) Dong, X.; Liu, C.; Fan, D.; Yu, Y.; Zhang, M. Insight into the effect of promoters (M=Cu, Ag, Zn, Zr) on aldol condensation reaction based on MgO surface in the process

of ethanol to 1, 3-butadiene: A comparative DFT study. *Applied Surface Science* **2019**, *481*, 576–587.

(29) Petitjean, H.; Guesmi, H.; Lauron-Pernot, H.; Costentin, G.; Loffreda, D.; Sautet, P.; Delbecq, F. How Surface Hydroxyls Enhance MgO Reactivity in Basic Catalysis: The Case of Methylbutynol Conversion. *ACS Catalysis* **2014**, *4*, 4004–4014.

(30) Da Ros, S.; Jones, M. D.; Mattia, D.; Schwaab, M.; Barbosa-Coutinho, E.; Rabelo-Neto, R. C.; Noronha, F. B.; Pinto, J. C. Microkinetic analysis of ethanol to 1,3-butadiene reactions over MgO-SiO_2 catalysts based on characterization of experimental fluctuations. *Chemical Engineering Journal* **2017**, *308*, 988–1000.

(31) Kozuch, S.; Shaik, S. How to Conceptualize Catalytic Cycles? The Energetic Span Model. *Accounts of Chemical Research* **2011**, *44*, 101–110.

(32) Shylesh, S.; Bettinson, L. A.; Aljahri, A.; Head-Gordon, M.; Bell, A. T. Experimental and Computational Studies of Carbon-Carbon Bond Formation via Ketonization and Aldol Condensation over Site-Isolated Zirconium Catalysts. *ACS Catalysis* **2020**, *10*, 4566–4579.

(33) Garay-Ruiz, D.; Bo, C. Revisiting Catalytic Cycles: A Broader View Through the Energy Span Model. *ACS Catalysis* **2020**, *10*, 12627–12635.

(34) Taifan, W. E.; Li, Y.; Baltrus, J. P.; Zhang, L.; Frenkel, A. I.; Baltrusaitis, J. Operando Structure Determination of Cu and Zn on Supported MgO/SiO_2 Catalysts during Ethanol Conversion to 1,3-Butadiene. *ACS Catalysis* **2019**, *9*, 269–285.

(35) Kvisle, S.; Aguero, A.; Sneeden, R. Transformation of ethanol into 1,3-butadiene over magnesium oxide/silica catalysts. *Applied Catalysis* **1988**, *43*, 117–131.

(36) Chung, S.-H.; Angelici, C.; Hinterding, S. O.; Weingarth, M.; Baldus, M.; Houben, K.; Weckhuysen, B. M.; Bruijnincx, P. C. Role of Magnesium Silicates in Wet-Kneaded Sil-

ica–Magnesia Catalysts for the Lebedev Ethanol-to-Butadiene Process. *ACS Catalysis* **2016**, *6*, 4034–4045.

(37) Abdulrazzaq, H. T.; Rahmani Chokanlu, A.; Frederick, B. G.; Schwartz, T. J. Reaction Kinetics Analysis of Ethanol Dehydrogenation Catalyzed by MgO-SiO_2. *ACS Catalysis* **2020**, *10*, 6318–6331.

(38) Hayashi, Y.; Akiyama, S.; Miyaji, A.; Sekiguchi, Y.; Sakamoto, Y.; Shiga, A.; Koyama, T.-r.; Motokura, K.; Baba, T. Experimental and computational studies of the roles of MgO and Zn in talc for the selective formation of 1,3-butadiene in the conversion of ethanol. *Physical Chemistry Chemical Physics* **2016**, *18*, 25191–25209.

(39) Zhu, Q.; Wang, B.; Tan, T. Conversion of Ethanol and Acetaldehyde to Butadiene over MgO–SiO_2 Catalysts: Effect of Reaction Parameters and Interaction between MgO and SiO_2 on Catalytic Performance. *ACS Sustainable Chemistry & Engineering* **2017**, *5*, 722–733.

(40) Angelici, C.; Velthoen, M. E. Z.; Weckhuysen, B. M.; Bruijnincx, P. C. A. Influence of acid–base properties on the Lebedev ethanol-to-butadiene process catalyzed by SiO_2-MgO materials. *Catalysis Science & Technology* **2015**, *5*, 2869–2879.

(41) Kresse, G.; Hafner, J. Ab initio molecular dynamics for open-shell transition metals. *Physical Review B* **1993**, *48*, 13115–13118.

(42) Kresse, G.; Hafner, J. Ab initio molecular-dynamics simulation of the liquid-metal–amorphous-semiconductor transition in germanium. *Physical Review B* **1994**, *49*, 14251–14269.

(43) Kresse, G.; Furthmüller, J. Efficiency of ab-initio total energy calculations for metals and semiconductors using a plane-wave basis set. *Computational Materials Science* **1996**, *6*, 15–50.

(44) Kresse, G.; Furthmüller, J. Efficient iterative schemes for ab initio total-energy calculations using a plane-wave basis set. *Physical Review B* **1996**, *54*, 11169–11186.

(45) Blöchl, P. E. Projector augmented-wave method. *Physical Review B* **1994**, *50*, 17953–17979.

(46) Perdew, J. P.; Burke, K.; Ernzerhof, M. Generalized Gradient Approximation Made Simple. *Physical Review Letters* **1996**, *77*, 3865–3868.

(47) Heyden, A.; Bell, A. T.; Keil, F. J. Efficient methods for finding transition states in chemical reactions: Comparison of improved dimer method and partitioned rational function optimization method. *The Journal of Chemical Physics* **2005**, *123*, 224101.

(48) Henkelman, G.; Jónsson, H. A dimer method for finding saddle points on high dimensional potential surfaces using only first derivatives. *The Journal of Chemical Physics* **1999**, *111*, 7010–7022.

(49) Mills, G.; Jónsson, H.; Schenter, G. K. Reversible work transition state theory: application to dissociative adsorption of hydrogen. *Surface Science* **1995**, *324*, 305–337.

(50) Jónsson, H.; Mills, G.; Jacobsen, K. W. Nudged elastic band method for finding minimum energy paths of transitions. Classical and Quantum Dynamics in Condensed Phase Simulations. 1998; pp 385–404.

(51) Jensen, F. *Introduction to Computational Chemistry*, 3rd ed.; John Wiley & Sons, 2017.

(52) Campbell, C. T. Future Directions and Industrial Perspectives Micro- and macrokinetics: Their relationship in heterogeneous catalysis. *Topics in Catalysis* **1994**, *1*, 353–366.

(53) Campbell, C. T. The Degree of Rate Control: A Powerful Tool for Catalysis Research. *ACS Catalysis* **2017**, *7*, 2770–2779.

(54) Uhe, A.; Kozuch, S.; Shaik, S. Automatic analysis of computed catalytic cycles. *Journal of Computational Chemistry* **2011**, *32*, 978–985.

(55) Towns, J.; Cockerill, T.; Dahan, M.; Foster, I.; Gaither, K.; Grimshaw, A.; Hazlewood, V.; Lathrop, S.; Lifka, D.; Peterson, G. D.; Roskies, R.; Scott, J. R.; Wilkins-Diehr, N. XSEDE: Accelerating Scientific Discovery. *Computing in Science & Engineering* **2014**, *16*, 62–74.

Graphical TOC Entry